Atmospheric Environment 61 (2012) 48–55

Contents lists available at SciVerse ScienceDirect

Atmospheric Environment

journal homepage: www.elsevier.com/locate/atmosenv

Effects of building roof greening on air quality in street canyons

Jong-Jin Baik*, Kyung-Hwan Kwak, Seung-Bu Park, Young-Hee Ryu

School of Earth and Environmental Sciences, Seoul National University, Seoul 151-742, Republic of Korea

HIGHLIGHTS

- ► Building roof greening effects on air quality in street canyons are examined.
- ► Building roof greening is represented by specified cooling.
- ► Building roof greening improves near-road air quality.
- ► The degree of near-road air quality improvement increases as the cooling is strong.
- ► The degree of near-road air quality improvement depends on ambient wind direction.

ARTICLE INFO

Article history:
Received 6 February 2012
Received in revised form
7 May 2012
Accepted 22 June 2012

Keywords:
Building roof greening
Cooling
Air quality
Street canyon
CFD model

ABSTRACT

Building roof greening is a successful strategy for improving urban thermal environment. It is of theoretical interest and practical importance to study the effects of building roof greening on urban air quality in a systematic and quantitative way. In this study, we examine the effects of building roof greening on air quality in street canyons using a computational fluid dynamics (CFD) model that includes the thermodynamic energy equation and the transport equation of passive, non-reactive pollutants. For simplicity, building roof greening is represented by specified cooling. Results for a simple building configuration with a street canyon aspect ratio of one show that the cool air produced due to building roof greening flows into the street canyon, giving rise to strengthened street canyon flow. The strengthened street canyon flow enhances pollutant dispersion near the road, which decreases pollutant concentration there. Thus, building roof greening improves air quality near the road. The degree of air quality improvement near the road increases as the cooling intensity increases. In the middle region of the street canyon, the air quality can worsen when the cooling intensity is not too strong. Results for a real urban morphology also show that building roof greening improves air quality near roads. The degree of air quality improvement near roads due to building roof greening depends on the ambient wind direction. These findings provide a theoretical foundation for constructing green roofs for the purpose of improving air quality near roads or at a pedestrian level as well as urban thermal environment. Further studies using a CFD model coupled with a photochemistry model and a surface energy balance model are required to evaluate the effects of building roof greening on air quality in street canyons in a more realistic framework.

1. Introduction

Air pollution and urban heat islands are atmospheric phenomena experienced by most large cities. Extensive studies have been performed to understand the physics and chemistry of air pollution and the meteorological and environmental aspects of urban heat islands. Many studies have been attempted to find and evaluate practical approaches that could mitigate urban heat islands, especially on hot summer days, and improve urban air quality. Reviews of these research subjects are available (Taha, 1997; Arnfield, 2003; Vardoulakis et al., 2003; Ravindra et al., 2008; Kumar et al., 2011).

In a recent decade, green roofs consisting of grasses, flowers, and/or other plants have become popular in city planning. The green roof system is one approach that could help to improve urban thermal environment (mitigate urban heat islands). It is well-known that the air temperature near a green roof is lower than that near an impervious roof that is composed of concrete, brick, or other impervious materials. In the daytime, cool air is produced beneath vegetation canopies at a green roof because less solar radiation is absorbed by the roof surface, so-called the shading effect of vegetation. Fioretti et al. (2010) observed that the monthly

* Corresponding author. Tel.: +82 2 880 6990; fax: +82 2 883 4972.
E-mail address: jjbaik@snu.ac.kr (J.-J. Baik).

1352-2310/$ – see front matter © 2012 Elsevier Ltd. All rights reserved.
http://dx.doi.org/10.1016/j.atmosenv.2012.06.076

average global radiation in the hot season is reduced by ~90% beneath vegetation canopies as compared with that above vegetation canopies at a green roof in Italy. One of the important changes in the energy balance of a green roof is a conversion of available net radiation into latent heat flux by evaporation from the soil surface and/or transpiration by plants of a green roof. This contributes to the decrease in air temperature near a green roof. Takebayashi and Moriyama (2007) observed that the daily average sensible heat flux in summertime from a green roof is lower by 70 W m^{-2} than that from a concrete roof. A study that employs an energy balance model indicated that green roofs have less sensible heat and heat storage than bare roofs and that the soil water availability is an important factor in regulating heat storage for green roofs (Tsang and Jim, 2011).

A study of field measurements in Singapore showed that the decrease in air temperature near a building roof can be up to 5 °C due to a green roof (Hien et al., 2007). Using a two-dimensional microscale model, Alexandria and Jones (2008) examined the effects of covering the building envelope with vegetation on thermal environment in urban canopies. They showed that when the roofs are covered with vegetation, much cooler air by 5–13 °C on average in the daytime flows into canyons from the vegetated roofs. The effects of cooling due to green roofs on urban air quality were not examined in their study. Several studies have shown that green roofs can contribute to improving air quality in urban areas by highlighting the own effects of vegetation such as the uptake of gaseous pollutants through stomata and the interception of particulate matter with leaves (dry deposition) (e.g., Currie and Bass, 2008; Yang et al., 2008; Rowe, 2011). These studies did not examine the effects of cooling due to green roofs on urban air quality. The lack of systematic and quantitative investigations of the effects of cooling due to green roofs on urban air quality motivates our present study.

Thermal effects on flow and pollutant dispersion in street canyons have been widely investigated. However, previous studies have almost exclusively examined the effects of heating, specifically, the effects of street bottom or building wall heating by solar radiation (Sini et al., 1996; Li et al., 2010). Li et al. (2010) emphasized that street bottom heating significantly enhances mean flow and turbulence in a street canyon and therefore facilitates pollutant removal from the street canyon. The effects of cooling due to green roofs on flow and pollutant dispersion in street canyons need to be studied. A comparison between cooling and heating effects would be of interest as it may reveal similarities in the fluid dynamics of the two scenarios. This also motivates our present study.

This study aims to examine the effects of building roof greening on air quality in street canyons. To achieve this, a computational fluid dynamics (CFD) modeling approach is employed and building roof greening is represented by cooling building roof and the air just above it. The numerical model used in this study is briefly described in Section 2. In Section 3, an experimental design in a simple building configuration is described and results are presented and discussed. In Section 4, an experimental design in a real urban morphology is described and results are presented and discussed. A summary and conclusions are presented in Section 5.

2. Model description and validation

The CFD model used in this study is a Reynolds-averaged Navier–Stokes equations (RANS) model that includes the renormalization group (RNG) $k-\varepsilon$ turbulence closure scheme (Baik et al., 2003, 2007; Kim and Baik, 2004). The governing equations consist of the momentum equation, mass continuity equation, thermodynamic energy equation, and scalar transport equation. Following Versteeg and Malalasekera (1995), wall boundary conditions for momentum and heat are used at the solid surface. The governing equations are solved numerically using the finite volume method. For details of the CFD model, see the references cited above.

The CFD model was validated against datasets from wind tunnel experiments by Meroney et al. (1996), Brown et al. (2000), and Uehara et al. (2000). Validation results demonstrated that the CFD model performs well in reproducing velocities, temperatures, and scalar concentrations in and above street canyons (Baik et al., 2003, 2007; Kim and Baik, 2004). Another validation test is performed using CODASC (concentration data of street canyons) dataset from the wind tunnel experiment of Gromke et al. (2008). Fig. 1 shows the scatter plot of normalized concentrations of the wind tunnel experiment and the numerical simulation. 35 locations that are uniformly distributed in the vicinity of the upwind building wall are selected for validation. The simulated concentration is quite well correlated with the measured concentration, showing R^2 of 0.95. Fig. 1 demonstrates the accuracy of the CFD model for simulating scalar dispersion in a street canyon.

3. Simple building configuration

3.1. Experimental design

First, we examine building roof greening effects in a simple framework. For this, an infinitely long street canyon configuration is considered. Fig. 2 depicts computational domain and the configuration of two buildings with equal height and a street canyon. The origin of the coordinate system is the center of the street bottom. The ambient (inflow) wind blows perpendicular to the street canyon axis. The computational domain size is 50 m in the x-direction (streamwise) and y-direction (spanwise) and 60.8 m in the z-direction. Both the building height (H) and the width between the two buildings (W) are 20 m, which gives a street canyon aspect ratio of one ($H/W = 1$). The computational domain in the x-direction ranges from $x/H = -1.5$ to 1. The grid size is 0.5 m in the x-direction and 1 m in the y-direction. The grid size in the z-direction is 0.5 m up to $z = 31.5$ m, and above this height it gradually increases with an expansion ratio of 1.1. The CFD model is integrated for 2 h with a time step of 0.1 s. The initial air temperature is set to 30 °C. The temperature of the upwind building roof

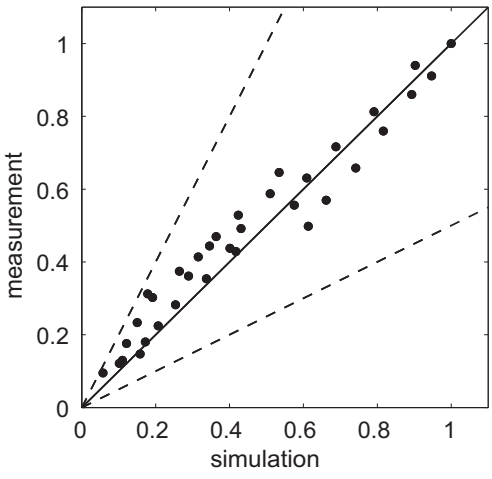

Fig. 1. Scatter plot of measured and simulated concentrations normalized by their maximum values at $z/H = 0.025$ and $y/H = -0.5$ (H: building height). Considering the symmetry of the concentration field in the wind tunnel experiment of Gromke et al. (2008), concentrations at 35 locations from $y/H = -4.5$ to -0.5 in the vicinity of the upwind building wall are plotted. Solid and two dashed lines are 1:1, 2:1, and 1:2 lines, respectively.

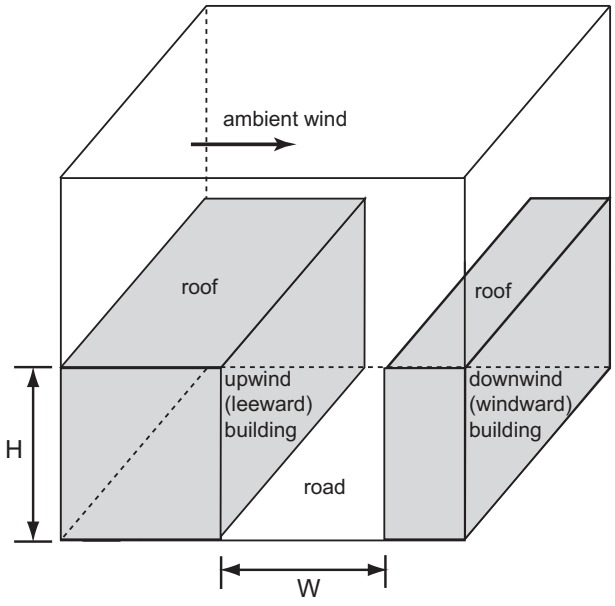

Fig. 2. Computational domain and the configuration of two buildings and a street canyon.

and the air temperature at the first model level above the upwind building roof ($z = H + 0.25$ m) are specified. Seven numerical experiments are performed with different specified temperatures, ranging from 30 to 18 °C in 2 °C intervals. That is, the cooling intensity is 0, 2, 4, 6, 8, 10, and 12 °C in these seven numerical experiments. The upwind and downwind building wall temperatures, downwind building roof temperature, and road temperature are set to 30 °C. The inflow wind profile is logarithmic, with the inflow wind speed at $z = H$ being 2.0 m s^{-1}. The calculated Reynolds number in the simulations is $\sim 2.5 \times 10^6$. An area source of passive, non-reactive pollutants is considered. There is no pollutant emission for the first 30 min. Then, starting from $t = 30$ min, pollutants are continuously emitted from the lowest model level ($z = 0.25$ m) with an emission rate of 10 ppb s^{-1} per grid point. The emission rate is equivalent to 3.2 μg s^{-1} per grid point when pollutants are regarded as NO_x with a NO-to-NO_2 ratio of 9:1.

3.2. Results and discussion

Fig. 3 shows the street canyon- and time-averaged air temperature as a function of cooling intensity. In this study, the time average is taken from $t = 90$ to 120 min. While the cooling is steadily applied, the street canyon-averaged air temperature reaches a quasi-steady state after a certain period of time. As expected, the average air temperature decreases with increasing cooling intensity. This is because cooler air flows into the street canyon as the cooling becomes stronger. The average air temperature is 28.5 °C for a cooling intensity of 6 °C and 26.7 °C for a cooling intensity of 12 °C. The average air temperature for the whole computational domain is also calculated. It is 29.3 °C for a cooling intensity of 6 °C and 28.6 °C for a cooling intensity of 12 °C.

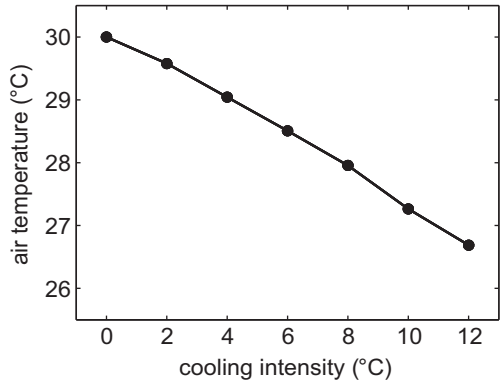

Fig. 3. Street canyon- and time-averaged air temperature as a function of cooling intensity.

The along-canyon- and time-averaged streamline and air temperature fields in the case of a cooling intensity of 6 °C are shown in Fig. 4. A clockwise-rotating primary vortex and a counterclockwise-rotating secondary corner vortex are formed in the street canyon (Fig. 4a). The center of the primary vortex in the vertical ($z/H = 0.40$) is located below the center of the street canyon. This contrasts with the case of street bottom heating in which the center of the primary vortex in the vertical is located above the center of the street canyon (Baik et al., 2007). The air temperature field (Fig. 4b) implies that the cool air flows into the street canyon. The cool air distribution in the street canyon is largely associated with the circulation of the primary vortex. An intrusion of the cool air into the street canyon near the upwind building wall is somewhat prevented due to the upward motion there.

The cool air that was produced near the upwind building roof and intruded into the street canyon can affect the intensity of street canyon flow. To study this, the street canyon- and time-averaged mean and turbulent kinetic energies are calculated (Fig. 5). Both the average mean kinetic energy and turbulent kinetic energy increase as the cooling intensity increases. When the cooling is stronger than 2 °C, the increasing rate of the average mean kinetic energy with cooling intensity is larger than that of the average

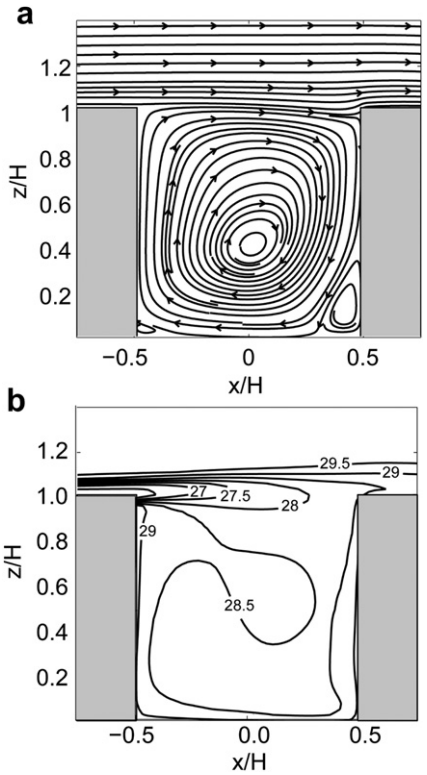

Fig. 4. Along-canyon- and time-averaged (a) streamline and (b) air temperature fields for a cooling intensity of 6 °C. The unit of air temperature in (b) is °C.

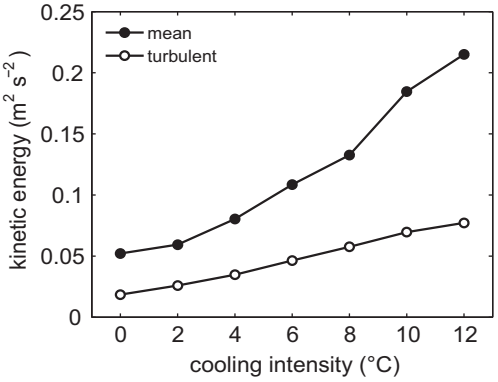

Fig. 5. Street canyon- and time-averaged mean kinetic energy and turbulent kinetic energy as a function of cooling intensity.

turbulent kinetic energy. Fig. 5 indicates that the street canyon flow becomes stronger as the cooling intensifies. To be specific, the primary vortex strengthens with increasing cooling intensity. Below the center of the primary vortex, the along-canyon- and time-averaged maximum reversed streamwise velocity is 0.38, 0.33, 0.44, 0.47, 0.52, 0.53, and 0.54 m s^{-1} for cooling intensities of 0, 2, 4, 6, 8, 10, and 12 °C, respectively. Note that a primary vortex appears in all experiments. Fig. 5 also indicates that for a given cooling intensity the average mean kinetic energy is larger than the average turbulent kinetic energy. For a cooling intensity of 6 °C, the average mean kinetic energy (0.11 m^2 s^{-2}) is 2.2 times larger than the average turbulent kinetic energy (0.05 m^2 s^{-2}).

We have investigated reasons why the average turbulent kinetic energy increases with increasing cooling intensity (Fig. 5). For this, the shear production term and buoyancy production term in the turbulent kinetic energy equation were calculated. Analysis results showed that the shear production in the street canyon increases as the cooling intensity increases. This makes a contribution to the increase of turbulent kinetic energy. Analysis results also showed that the magnitude of the buoyancy production term is much smaller than that of the shear production term.

Many CFD modeling studies have characterized street canyon flow in the presence of street bottom or building wall heating for various street canyon aspect ratios (Sini et al., 1996; Kim and Baik, 1999; Li et al., 2010; Cheng and Liu, 2011). For a street canyon with an aspect ratio of one, a primary vortex is formed in the street canyon in the presence of upwind building wall or street bottom heating and the primary vortex is more intense than a primary vortex formed in the absence of heating. This is because the thermally (positive-buoyancy) driven upward motion near the upwind building wall is constructively combined with the mechanically driven upward motion there, accordingly producing more intense primary vortex. The present CFD modeling study indicates that in the presence of upwind building roof cooling the thermally (negative-buoyancy) driven downward motion is constructively combined with the mechanically driven downward motion, which strengthens vortex circulation. Therefore, the underlying fluid dynamics for the two different scenarios are similar as they both result in strengthened street canyon flow due to buoyancy effects.

Fig. 6a shows the street canyon- and time-averaged pollutant concentration as a function of cooling intensity. When there is cooling, the average pollutant concentration is lower than that in the no-cooling case. In other words, building roof greening improves air quality in the street canyon. The average pollutant concentration decreases as the cooling intensity increases. Fig. 6b shows the area- and time-averaged pollutant concentration as a function of cooling intensity at $z = 1.5$ m. The height of 1.5 m is approximately the height at which humans are exposed to harmful pollutants. It is obvious from Fig. 6b that the average pollutant concentration decreases with increasing cooling intensity. At a pedestrian level, more beneficial impact on human health would be expected with more enhanced green roofs.

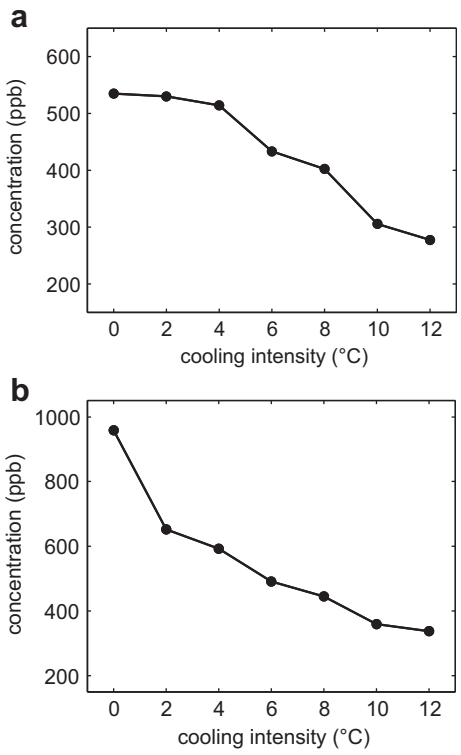

Fig. 6. (a) Street canyon- and time-averaged pollutant concentration as a function of cooling intensity and (b) area- and time-averaged pollutant concentration as a function of cooling intensity at $z = 1.5$ m.

It is interesting to note from Fig. 6 that in comparison with the no-cooling case the area- and time-averaged pollutant concentration at $z = 1.5$ m in the case of a cooling intensity of 2 °C is reduced by 32% from 958 to 652 ppb, but the street canyon- and time-averaged pollutant concentration is reduced by only 1% from 535 to 530 ppb. This implies that in some regions of the street canyon the pollutant concentration might be higher in the 2 °C cooling case than in the no-cooling case. To examine the decrease or increase of pollutant concentration with height in the street canyon due to the cooling in comparison with the no-cooling case, the reduction ratio of pollutant concentration at any height (R) is calculated using

$$R = -\frac{\overline{C} - \overline{C_0}}{\overline{C_0}}, \tag{1}$$

where $\overline{C_0}$ is the area- and time-averaged pollutant concentration in the no-cooling case and $\overline{C}$ is the area- and time-averaged pollutant concentration for a given cooling intensity. The vertical profiles of the reduction ratio for cooling intensities of 6, 8, and 10 °C are plotted in Fig. 7. Near the road, the reduction ratio is positive and high for all cooling intensities. Building roof greening improves air quality near the road, and the improvement becomes large as the cooling intensity increases. For a cooling intensity of 10 °C, the reduction ratio is positive at all heights of the street canyon. However, for cooling intensities of 6 and 8 °C, the reduction ratio is negative in the middle region of the street canyon. That is, the air quality worsens there.

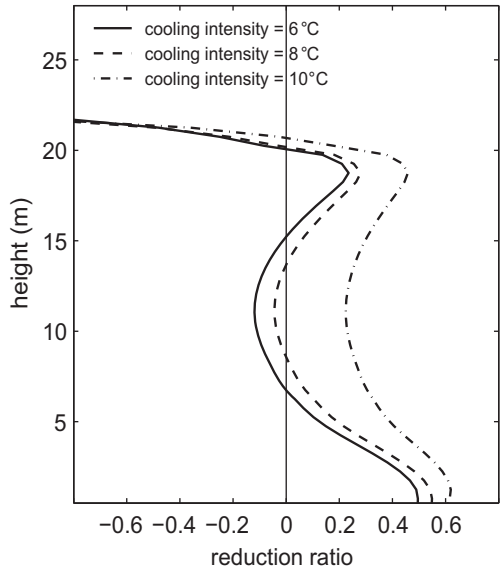

Fig. 7. Vertical profiles of the reduction ratio of area- and time-averaged pollutant concentration for cooling intensities of 6, 8, and 10 °C in comparison with the no-cooling case.

Figs. 5–7 demonstrate that the cooling due to green roofs causes air quality near the road to improve by strengthening street canyon flow and enhancing pollutant dispersion near the road when compared with the no-cooling case. Depending on the cooling intensity, pollutants can be less dispersed in the middle region of the street canyon. The less dispersion of pollutants, meaning higher pollutant concentration in a particular cooling case than in the no-cooling case, occurs when the cooling intensity is not too strong.

Fig. 8 shows along-canyon- and time-averaged pollutant concentration fields for cooling intensities of 0, 6, 8, and 10 °C. In all cases, the pollutant concentration is higher near the upwind building wall than near the downwind building wall. In the no-cooling case, the pollutant concentration is broadly low near the center of the street canyon. It is seen that the pollutant concentration in the vicinity of the center of the street canyon is lower in the no-cooling case than in the 6 and 8 °C cooling cases, making a contribution to the negative reduction ratios in the middle region of the street canyon in the 6 and 8 °C cooling cases (Fig. 7). The pollutant concentration near the upwind building wall is much lower in the 10 °C cooling case than in the no-cooling case, making a contribution to the positive reduction ratio in the 10 °C cooling case (Fig. 7).

Some of pollutants emitted from the street bottom escape from the street canyon. To examine the mechanism responsible for pollutant escape from the street canyon under different cooling intensities, the vertical mean flux of pollutants (F_m) and the vertical turbulent flux of pollutants (F_t) at the level of the building roof ($z = H$) are calculated using the following equations by Baik and Kim (2002).

$$F_m = CW, \tag{2}$$

$$F_t = \overline{cw} = -K_c \frac{\partial C}{\partial z}, \tag{3}$$

where C is the mean pollutant concentration, W is the mean vertical velocity, c is the deviation from the mean pollutant concentration,

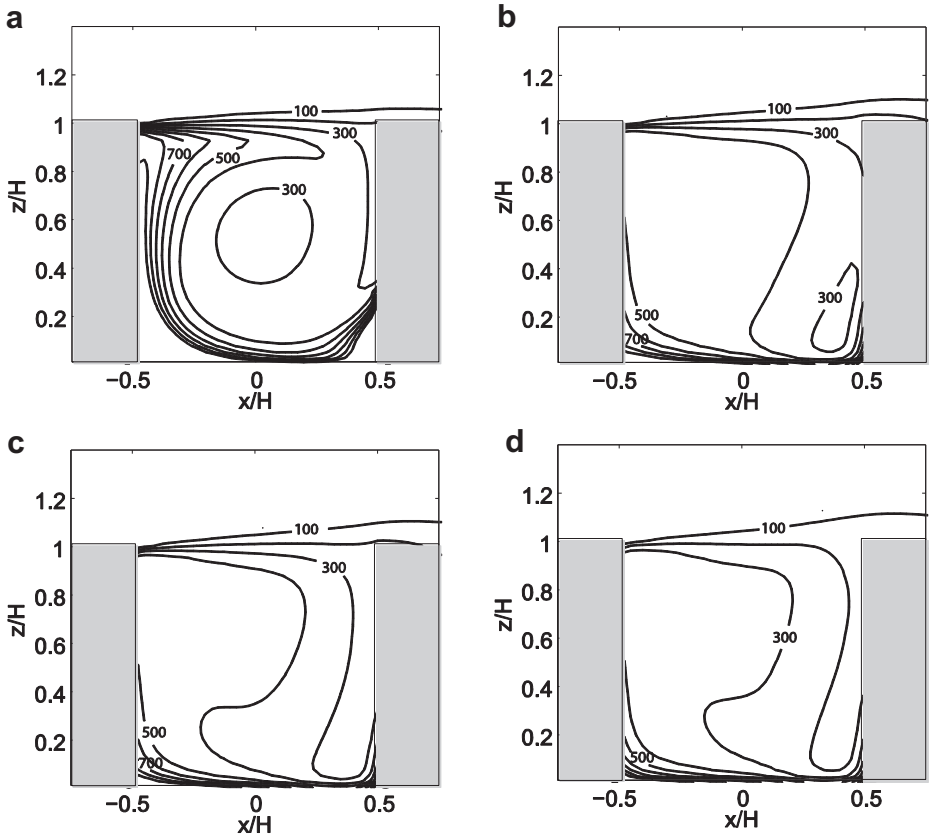

Fig. 8. Along-canyon- and time-averaged pollutant concentration fields for cooling intensities of (a) 0, (b) 6, (c) 8, and (d) 10 °C. The contour intervals are 100 ppb, and contours larger than 900 ppb are not plotted for clarity of figure.

w is the deviation from the mean vertical velocity, and K_c is the turbulent eddy diffusivity of pollutants.

Fig. 9 shows the area-integrated and time-averaged vertical mean and turbulent fluxes of pollutants at $z = H$. The direction of the positive pollutant fluxes is upward. The vertical mean flux is negligibly small for cooling intensities of 0 and 2 °C, shows a large increase between 2 and 4 °C, and does not change much between 4 and 12 °C. The vertical turbulent flux decreases as the cooling intensity increases. For very weak cooling, the vertical turbulent flux is much larger than the vertical mean flux. For strong cooling, the two vertical fluxes become comparable in magnitude, that is, both the mean and turbulent flows play important roles in removing pollutants from the street canyon.

In the present simple building configuration, only a street canyon with an aspect ratio of one is considered. It is known that the number of vortices formed in a street canyon depends on the street canyon aspect ratio (Jeong and Andrews, 2002; Cheng et al., 2008). Hence, interesting street canyon flow patterns are expected when the cool air flows into street canyons with larger street canyon aspect ratios where two or three vortices would be produced in the absence of thermal forcing. Examining the effects of building roof greening on air quality in street canyons for a wide range of street canyon aspect ratios would be an interesting direction for future work.

4. Real urban morphology

4.1. Experimental design

Next, we examine building roof greening effects in a real urban morphology. For this, a central region of Seoul, Korea is selected (Fig. 10a). A larger region than this one was chosen for a study of urban flow and dispersion using a CFD model coupled with a mesoscale model (Baik et al., 2009). The grid size is 4 m in both the x-direction (east–west) and y-direction (north–south). The grid size in the z-direction is 2 m up to $z = 112$ m and then increases with an expansion ratio of 1.1 up to the model top boundary. The computational domain size is 392, 392, and 159 m in the x-, y-, and z-direction, respectively. The time step used is 0.2 s, and the CFD model is integrated for 2 h. The initial air temperature is set to 30 °C. The temperature of all building roofs and the air temperature at the first model level above each building roof (z = each building height + 1 m) are set to 25 °C. Thus, the cooling intensity is 5 °C. The temperatures of all building walls and roads are set to 30 °C. A westerly inflow is considered, and the inflow profile is the same as that used in the simple building configuration experiments. For the first 30 min, no pollutants are emitted. Starting from $t = 30$ min, pollutants are continuously emitted from all grid points at the lowest model level ($z = 1$ m) except for grid points right adjacent to building walls. An emission rate is 1 ppb s^{-1} per grid point. For analysis, a smaller area with 320 m in both the x- and y-direction is taken to reduce lateral boundary effects. In the smaller area, the fractional building coverage at the surface is 0.42 (Fig. 10b) and the maximum building height is 80 m.

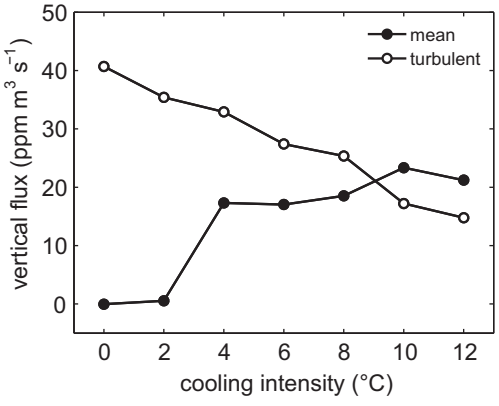

Fig. 9. Area-integrated and time-averaged vertical mean and turbulent fluxes of pollutants at the level of the building roof.

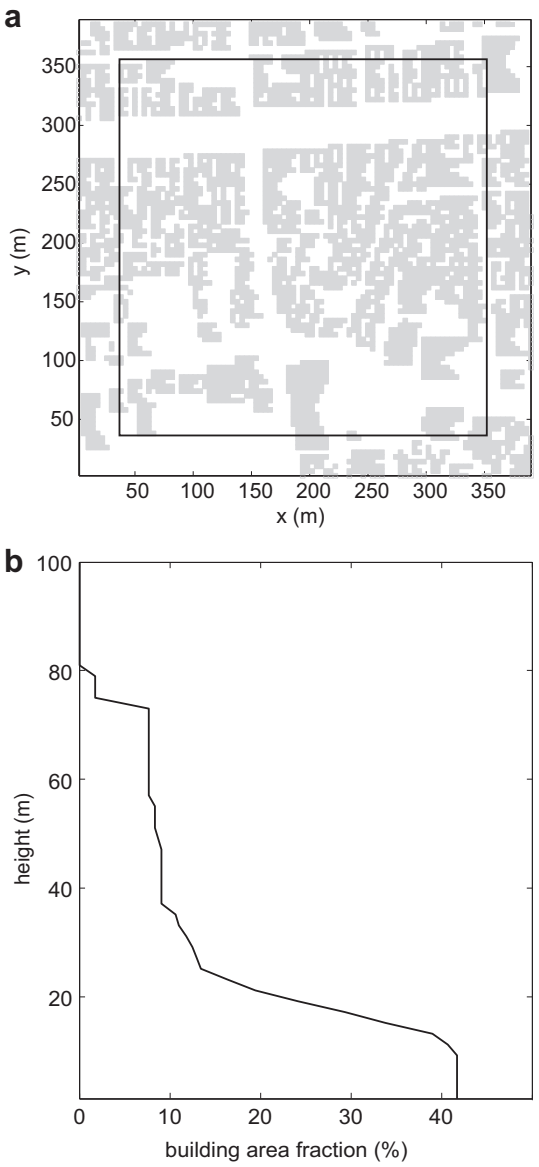

Fig. 10. (a) Building configuration in a computational domain and (b) the vertical profile of building area fraction for a real urban morphology. Experimental results inside the solid line in Fig. 10a are analyzed.

4.2. Results and discussion

Fig. 11 shows pollutant concentration fields at $z = 1.5$ m and $t = 120$ min in the no-cooling case and 5 °C cooling case. The pollutant concentration is reduced when the cooling is present. The area-averaged pollutant concentration is 292 ppb in the no-cooling case and 131 ppb in the 5 °C cooling case.

Fig. 12 shows the vertical profiles of area- and time-averaged air temperature in the 5 °C cooling case and the reduction ratio of

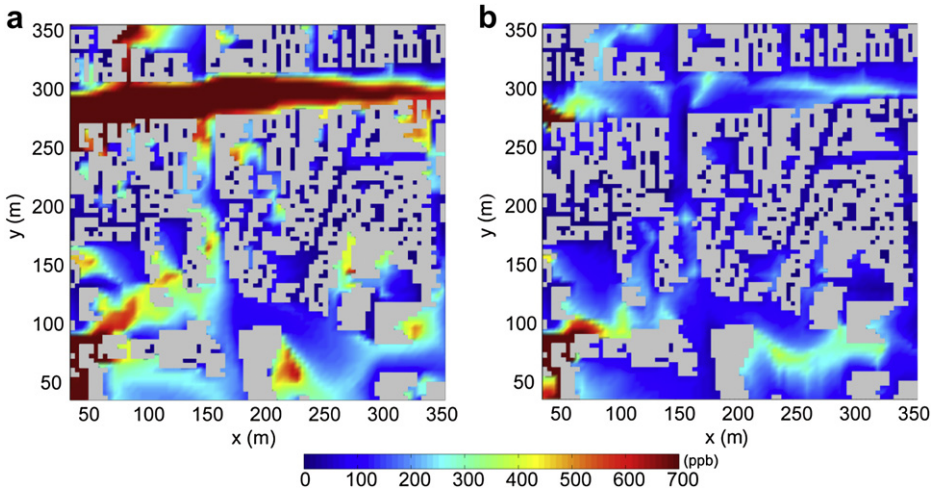

Fig. 11. Pollutant concentration fields at $z = 1.5$ m and $t = 120$ min in the (a) no-cooling case and (b) 5 °C cooling case in a real urban morphology. Buildings are gray-shaded.

pollutant concentration in the 5 °C cooling case in comparison with the no-cooling case. The average air temperature decreases up to $z = 15$ m and then overall increases with height. Above $z = 89$ m, the average air temperature is 30 °C. It is interesting to see that the lowest average air temperature occurs at the height ($z = 15$ m) where the area fraction of building roofs is large. The reduction ratio is positive below $z = 18$ m (reduced pollutant concentration) but negative from $z = 18$ to 62 m (enhanced pollutant concentration).

To get some insight of flow and pollutant concentration, the spatial- and time-averaged horizontal wind speed and upward vertical velocity are calculated. Here, the vertical extent of spatial average is taken from $z = 0$ to 18 m. The average horizontal wind speed is 0.77 m s^{-1} in the no-cooling case and 0.58 m s^{-1} in the 5 °C cooling case. In contrast, the average upward vertical velocity is 0.07 m s^{-1} in the no-cooling case and 0.11 m s^{-1} in the 5 °C cooling case. The horizontal flow is weaker and the upward flow is stronger in the 5 °C cooling case. The strengthened upward flow around buildings in the 5 °C cooling case makes a contribution to the enhanced dispersion of pollutants, which results in lower pollutant concentrations below $z = 18$ m and higher pollutant concentrations between $z = 18$ and 62 m.

To examine the dependence of building roof greening effects on the ambient (inflow) wind direction, numerical experiments are performed with eight ambient wind directions: westerly (W), north-westerly (NW), northerly (N), north-easterly (NE), easterly (E), south-easterly (SE), southerly (S), and south-westerly (SW). Fig. 13 shows area- and time-averaged pollutant concentrations at $z = 1.5$ m in the no-cooling case and 5 °C cooling case. All numerical experiments demonstrate the positive effect of building roof greening on pollutant dispersion near roads. On average for the eight experiments, the average pollutant concentration is reduced by 49% from 247 to 126 ppb. The largest reduction (57%) occurs for the north-westerly inflow showing the highest concentration in the no-cooling case. On the other hand, the smallest reduction (30%) occurs for the southerly inflow showing the lowest concentration in the no-cooling case. The variation of pollutant concentration with the ambient wind direction is smaller in the 5 °C cooling case than in the no-cooling case. This indicates weaker dependence of

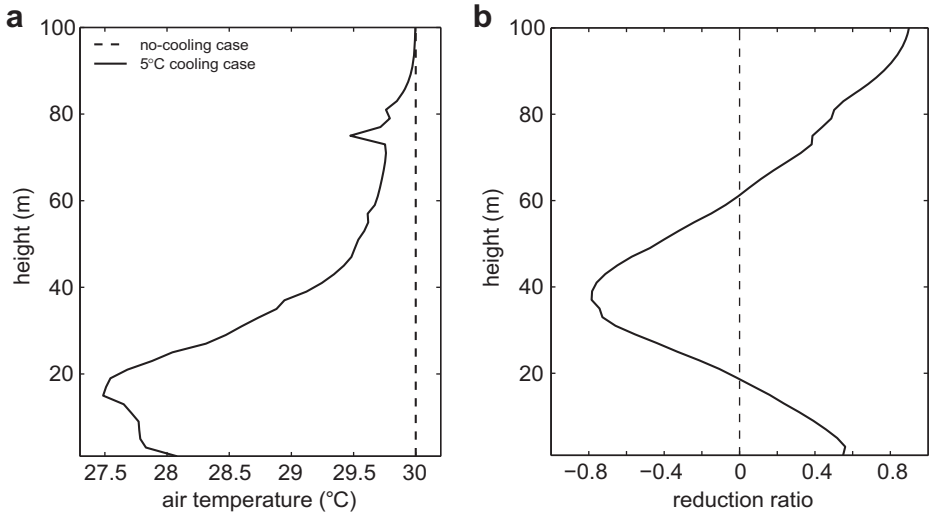

Fig. 12. Vertical profiles of (a) area- and time-averaged air temperature in the 5 °C cooling case and (b) the reduction ratio of pollutant concentration in the 5 °C cooling case in comparison with the no-cooling case.

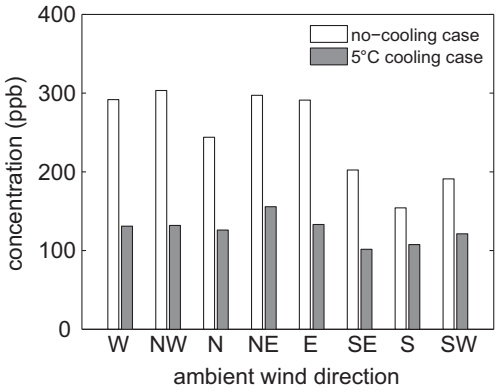

Fig. 13. Area- and time-averaged pollutant concentrations at $z = 1.5$ m for eight ambient wind directions in the no-cooling case and 5 °C cooling case.

pollutant concentration on the ambient wind direction when building roof greening exists.

5. Summary and conclusions

We examined the effects of building roof greening, which is represented by specified cooling, on air quality in street canyons using a CFD model. It was shown for a simple building configuration with a street aspect ratio of one that the cool air produced due to building roof greening flows into the street canyon and results in strengthened street canyon flow. The strengthened street canyon flow enhances pollutant dispersion near the road, thereby decreasing pollutant concentration and hence improving air quality near the road. The degree of air quality improvement near the road increases with increasing cooling intensity. It was also shown for a real urban morphology that building roof greening improves air quality near roads. The degree of air quality improvement near roads depends on the ambient wind direction. Further work is required to investigate whether the finding in this study holds for other building configurations (such as a finitely long street canyon configuration and an array of cubical buildings) and other real urban morphologies.

In this study, passive, non-reactive pollutants were considered. In reality, urban pollutants are reactive and photochemical reactions during the day are affected by air temperature. Thus, the cool air that flows into a street canyon due to building roof greening may affect the amount of secondary photochemical pollutants produced. To examine dynamical (in this study) and chemical effects together, a CFD model coupled with a photochemistry model is needed. We will investigate this in future. In this study, building roof greening was represented by specified cooling. This restriction could be relaxed by implementing a surface energy balance model that includes vegetation in the CFD model.

Acknowledgements

The authors are grateful to two anonymous reviewers for providing valuable comments on this work. This work was supported by the National Research Foundation of Korea (NRF) grant funded by the Korea Ministry of Education, Science and Technology (MEST) (No. 2011-0017041).

References

Alexandria, E., Jones, P., 2008. Temperature decreases in an urban canyon due to green walls and green roofs in diverse climates. Building and Environment 43, 480–493.
Arnfield, A.J., 2003. Two decades of urban climate research: a review of turbulence, exchanges of energy and water, and the urban heat island. International Journal of Climatology 23, 1–26.
Baik, J.-J., Kim, J.-J., 2002. On the escape of pollutants from urban street canyons. Atmospheric Environment 36, 527–536.
Baik, J.-J., Kim, J.-J., Fernando, H.J.S., 2003. A CFD model for simulating urban flow and dispersion. Journal of Applied Meteorology 42, 1636–1648.
Baik, J.-J., Kang, Y.-S., Kim, J.-J., 2007. Modeling reactive pollutant dispersion in an urban street canyon. Atmospheric Environment 41, 934–949.
Baik, J.-J., Park, S.-B., Kim, J.-J., 2009. Urban flow and dispersion simulation using a CFD model coupled to a mesoscale model. Journal of Applied Meteorology and Climatology 48, 1667–1681.
Brown, M.J., Lawson Jr., R.E., DeCroix, D.S., Lee, R.L., 2000. Mean flow and turbulence measurements around a 2-D array of buildings in a wind tunnel. In: 11th Joint Conference on the Applications of Air Pollution Meteorology with the A&WMA, Long Beach, CA, USA, pp. 35–40.
Cheng, W.C., Liu, C.-H., 2011. Large-eddy simulation of turbulent transports in urban street canyons in different thermal stabilities. Journal of Wind Engineering and Industrial Aerodynamics 99, 434–442.
Cheng, W.C., Liu, C.-.H., Leung, D.Y.C., 2008. Computational formulation for the evaluation of street canyon ventilation and pollutant removal performance. Atmospheric Environment 42, 9041–9051.
Currie, B.A., Bass, B., 2008. Estimates of air pollution mitigation with green plants and green roofs using the UFORE model. Urban Ecosystems 11, 409–422.
Fioretti, R., Palla, A., Lanza, L.G., Principi, P., 2010. Green roof energy and water related performance in the Mediterranean climate. Building and Environment 45, 1890–1904.
Gromke, C., Buccolieri, R., Di Sabatino, S., Ruck, B., 2008. Dispersion study in a street canyon with tree planting by means of wind tunnel and numerical investigations – evaluation of CFD data with experimental data. Atmospheric Environment 42, 8640–8650.
Hien, W.N., Yok, T.P., Yu, C., 2007. Study of thermal performance of extensive rooftop greenery systems in the tropical climate. Building and Environment 42, 25–54.
Jeong, S.J., Andrews, M.J., 2002. Application of the $k-\varepsilon$ turbulence model to the high Reynolds number skimming flow field of an urban street canyon. Atmospheric Environment 36, 1137–1145.
Kim, J.-J., Baik, J.-J., 1999. A numerical study of thermal effects on flow and pollutant dispersion in urban street canyons. Journal of Applied Meteorology 38, 1249–1261.
Kim, J.-J., Baik, J.-J., 2004. A numerical study of the effects of ambient wind direction on flow and dispersion in urban street canyons using the RNG $k-\varepsilon$ turbulence model. Atmospheric Environment 38, 3039–3048.
Kumar, P., Ketzel, M., Vardoulakis, S., Pirjola, L., Britter, R., 2011. Dynamics and dispersion modelling of nanoparticles from road traffic in the urban atmospheric environment–a review. Journal of Aerosol Science 42, 580–603.
Li, X.-X., Britter, R.E., Koh, T.Y., Norford, L.K., Liu, C.-H., Entekhabi, D., Leung, D.Y.C., 2010. Large-eddy simulation of flow and pollutant transport in urban street canyons with ground heating. Boundary-Layer Meteorology 137, 187–204.
Meroney, R.N., Pavageau, M., Rafailidis, S., Schatzmann, M., 1996. Study of line source characteristics for 2-D physical modeling of pollutant dispersion in street canyons. Journal of Wind Engineering and Industrial Aerodynamics 62, 37–56.
Ravindra, K., Sokhi, R., Van Grieken, R., 2008. Atmospheric polycyclic aromatic hydrocarbons: source attribution, emission factors and regulation. Atmospheric Environment 42, 2895–2921.
Rowe, D.B., 2011. Green roofs as a means of pollution abatement. Environmental Pollution 159, 2100–2110.
Sini, J.-F., Anquetin, S., Mestayer, P.G., 1996. Pollutant dispersion and thermal effects in urban street canyons. Atmospheric Environment 30, 2659–2677.
Taha, H., 1997. Urban climates and heat islands: albedo, evapotranspiration, and anthropogenic heat. Energy and Buildings 25, 99–103.
Takebayashi, H., Moriyama, M., 2007. Surface heat budget on green roof and high reflection roof for mitigation of urban heat island. Building and Environment 42, 2971–2979.
Tsang, S.W., Jim, C.Y., 2011. Theoretical evaluation of thermal and energy performance of tropical green roofs. Energy 36, 3590–3598.
Uehara, K., Murakami, S., Oikawa, S., Wakamatsu, S., 2000. Wind tunnel experiments on how thermal stratification affects flow in and above urban street canyons. Atmospheric Environment 34, 1553–1562.
Vardoulakis, S., Fisher, B.E.A., Pericleous, K., Gonzalez-Flesca, N., 2003. Modelling air quality in street canyons: a review. Atmospheric Environment 37, 155–182.
Versteeg, H.K., Malalasekera, W., 1995. An Introduction to Computational Fluid Dynamics: The Finite Volume Method. Longman, Malaysia, pp. 198–203.
Yang, J., Yu, Q., Gong, P., 2008. Quantifying air pollution removal by green roofs in Chicago. Atmospheric Environment 42, 7266–7273.